

The rate of cosmic ray showers at large zenith angles: a step towards the detection of ultra-high energy neutrinos by the Pierre Auger Observatory

M. Ave, R.A. Vázquez, and E. Zas

*Departamento de Física de Partículas,
Universidad de Santiago, 15706 Santiago de Compostela, Spain*

J.A. Hinton and A.A. Watson

*Department of Physics and Astronomy
University of Leeds, Leeds LS2 9JT, UK*

Abstract

It is anticipated that the Pierre Auger Observatory can be used to detect cosmic neutrinos of $> 10^{19}$ eV that arrive at very large zenith angles. However showers created by neutrino interactions close to the detector must be picked out against a background of similar events initiated by cosmic ray nuclei. As a step towards understanding this background, we have made the first detailed analysis of air showers recorded at Haverah Park (an array which used similar detectors to those planned for the Auger Observatory) with zenith angles above 60° . We find that the differential shower rate from 60° to 80° can be predicted accurately when we adopt the known primary energy spectrum above 10^{17} eV and assume the QGSJET model and proton primaries. Details of the calculation are given.

1 Introduction

Horizontal air showers have been studied for many years for several different reasons [1, 2, 3]. Much of the relevance of horizontal air showers induced by cosmic rays is in the understanding of the background against which high energy neutrino showers could be detected. Although no neutrino events can be expected in the Haverah Park data set, even for the most optimistic neutrino flux predictions, it has recently been shown that relevant bounds could be obtained with the Auger Observatories [4, 5].

Horizontal cosmic ray showers are of great interest in their own right for two principle reasons. Firstly the acceptance of an air-shower array could be doubled if events above 60° can be adequately analysed. Secondly because, uniquely, they deal with surviving particles that are created very close to the shower core, they complement the information obtained in the study of near vertical cosmic ray showers. Moreover understanding the azimuthal asymmetries at large zenith angles [6,7,8,9,10 (hereafter Paper I)] can lead to significant improvement of ultra high energy shower analysis at moderate zenith angles ($30^\circ - 60^\circ$) [11].

The Haverah Park array, being made of 1.2 m deep water-Čerenkov tanks [12], is quite possibly the array detector so far constructed which is best suited on geometrical considerations for the analysis of very large inclined showers. Moreover it can be considered as an early prototype of the Auger Observatories which will employ water-Čerenkov tanks of identical depth. The quantitative aspects of our results are very specific to the water-Čerenkov technique.

During the 14 years of operation of the Haverah Park array [13] which are considered here nearly 10000 air showers were recorded for $\theta > 60^\circ$. The analysis of these data was difficult because of the complex geomagnetic field effects which distort the circular symmetry of air showers, the relatively small size of the array (12 km²) and the limited computing power then available, both for data analysis and simulation. A single remarkable event, perhaps of 10^{20} eV, at 85° from the zenith which triggered 20 of the array detectors was extensively discussed [7], but no systematic study was made with those data for which the initial analysis gave a zenith angle $\theta > 60^\circ$.

Here we present the results of the first systematic analysis of horizontal showers from primaries of energy greater than 10^{17} eV at Haverah Park with zenith angles exceeding 60° , comparing them to those expected from the known cosmic ray spectrum. Preliminary results of this work were reported in [14]. For the calculation of the expected rates we make use of a parameterization for the muon number densities at ground level described elsewhere (Paper I). We take into account two possible compositions (proton and iron nuclei) and use alternative models for the high energy interactions namely QGSJET [15] and SIBYLL 1.6 [16].

The article is organized as follows: In section 2 we discuss the relative signals and fluctuations expected from the electromagnetic (electrons and photons) and muon components in horizontal air showers (HAS) induced by hadrons and in section 3 we address the muon component of HAS. In section 4 we discuss the detector simulation paying particular attention to the origin of the different parts of the signal from the individual tanks, stressing the differences between vertical and horizontal particle signals. In section 5 we describe in detail the procedure implemented to obtain a prediction for the horizontal shower rate and in section 6 we give the results obtained in the different cases. Our conclusions are presented in section 7.

2 Muon and Electromagnetic Components in Horizontal Air Showers

An air shower induced by a proton or a nucleus can be qualitatively understood as a pion shower that is continuously feeding an electromagnetic component (photons, electrons, and positrons) through π^0 decay, and both a muonic and a neutrino component through charged pion decay. At ground

level the typical number density ratio of photons to electrons in a vertical shower is stable. For a low energy threshold of 90 keV this ratio has a value typically between 20 : 1 and 30 : 1 for proton or iron as the distance to shower axis r changes from 100 m to 1 km. This value is characteristic of electromagnetic showers. The ratio of electrons to muons on the other hand depends strongly on r . For example for a 10^{19} eV proton shower it drops from $\sim 100 : 1$ to $\sim 3 : 1$ as r rises in the same interval.

In spite of outnumbering the muon component, the average electron and photon energies are typically in the few MeV range, compared to GeV and above for muons. As a result the relative contributions to the signal in a water-Čerenkov tank are not so different because the water-Čerenkov technique is on average much more efficient at converting single muons into signals than electrons or photons.

Direct measurements with Fly’s Eye [17] have shown that above 10^{17} eV the shower maximum is usually between 600 g cm^{-2} and sea level ($\sim 1000 \text{ g cm}^{-2}$). As the zenith angle varies from the vertical, $\theta = 0^\circ$, to the horizontal, $\theta = 90^\circ$, direction, the slant matter depth rises to $\sim 36000 \text{ g cm}^{-2}$ and showers are observed well past maximum. The behavior of the electromagnetic and muon components beyond shower maximum is shown in Fig. 1A. While the electromagnetic component of an air shower becomes exponentially attenuated with depth, the muons which do not decay propagate practically unattenuated to the ground, except for energy loss and geomagnetic deviations. As a result the ratio of the electromagnetic to the muon component of an air shower drops as the zenith angle increases up to 60° . Above this angle the ratio levels out because the muons themselves produce electromagnetic particles. The remaining electromagnetic component is mainly due to muon decay and to a smaller extent to hadronic interactions, pair production, and bremsstrahlung.

We have studied the effects of muon decay through Monte Carlo simulation using AIRES [18]. Indeed even at 60° the electromagnetic component of a 10^{19} eV proton shower which can be directly associated to π^0 decay is already low and confined within a relatively small region of about 200 m around shower axis. At higher zenith angles this component can be neglected and the muon decay contribution becomes stable, roughly at a proportion of 0.8 electrons for each muon, more than three times below the number obtained for vertical showers 1 km away from the shower axis. Unlike the electromagnetic component from pion decay in vertical showers, the lateral distribution follows that of the muons rather closely. This is not difficult to understand as the decay muons give rise to relatively small electromagnetic sub-showers that preserve the muon spatial distribution. The energy distribution of the electromagnetic component is essentially the same as that of an electromagnetic air shower (i.e. for vertical showers) for the same reason.

The contribution of muon interactions to the electromagnetic component can be simply estimated by considering the muon energy spectrum of a sin-

gle shower and folding it analytically with the bremsstrahlung cross section and the Greisen parameterization, see [19]. For an 80° zenith and 10^{19} eV proton shower the total number of electrons and positrons (N_e) obtained is about $2.5 \cdot 10^4$. These are mostly due to the muons in the energy range between 30 GeV and 500 GeV. As this component arises also from electromagnetic sub-showers its energy distribution should also reflect that of electromagnetic cascades. If we multiply, conservatively, the total number of electrons by a factor three to account for the two other muon interactions, it is still a factor of ~ 50 below the number of muons in the shower (see figure 1A).

The contribution to the signal from the electromagnetic component at high zenith angles is in the end small and dominated by muon decay. It has been simulated using WTANK [20] using the muon and electromagnetic signals from different zenith angle showers generated with AIRES [18] as an input. In Fig. 1B we show the simulated ratio of electromagnetic to muon signal in a Čerenkov tank of 1.2 m depth (as used in Haverah Park and planned for the Auger Observatory) as a function of distance to the shower axis for a vertical shower compared to two inclined showers. The shower particles have been fed through the tank simulation as if they were coming from the vertical direction to eliminate geometric tank effects. The results illustrate the genuine decrease in the electromagnetic to muon signal ratio due only to the shower composition varying with zenith angle. Even at distances from the shower axis of order ~ 1.5 km the ratio is about a factor 3 smaller than for vertical showers.

As will be shown in section 4, in the Haverah Park detectors the relative electromagnetic signal drops even further as the zenith angle increases because of geometric effects. At large zenith angles the muon track length is enhanced compared with that in the vertical direction and the output signal increases accordingly. In the analysis that follows we will consider a track dependent, but otherwise constant correction due to the electromagnetic component from muon decay, in agreement with [11], and neglect that from all muon interactions in the atmosphere.

3 The muon component of horizontal showers

The behavior of the muonic component at high zenith angles becomes extremely complex because of magnetic field effects. It is described in detail in Paper I where an accurate model is presented to account for the average muon number densities at ground level. The inputs for this model are the lateral distribution function (LDF), the average muon energy as a function of radius ($\mathcal{E}(r)$) and the mean distance to the muon production point, all evaluated in the absence of magnetic effects. The model is based on an anticorrelation between the average muon energy and distance of the muon

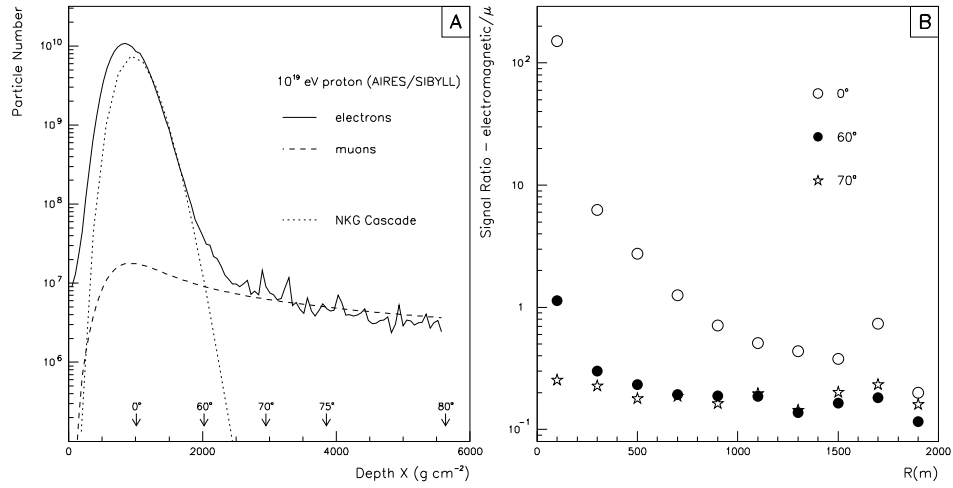


Figure 1: A) The longitudinal development of the muon and electron components averaged over 100, 10^{19} eV, showers. At depths exceeding 3000 g cm^{-2} , or equivalently for zenith angles greater than 70° , the electromagnetic component is mainly due to muon decay. B) The ratio of the electromagnetic to muon contributions to water-Cherenkov signal as a function of distance from the shower axis (see section 4 for details of the water tank simulation). The large scatter in the points beyond 1500 m is statistical.

from the core. We have generated these inputs, using AIRES, for two primaries proton and iron, and two hadronic models Quark Gluon String Model (QGSJET) and SIBYLL and for primary energies in the range 10^{16} eV to 10^{20} eV. The muon energy distribution at a fixed distance to the shower axis is assumed to have a log-normal distribution of width 0.4 (Paper I).

Both the $\mathcal{E}(r)$ and the shape of the LDF are essentially invariant over this large energy interval and only mildly dependent on zenith angle as shown in Fig. 2. As a result the dependence on shower energy of the muon number density distributions with the magnetic field can be parameterized with an absolute normalization to a high level of precision. The dependence of the normalization factor with energy can be obtained by monitoring the total muon number in the showers. The results are plotted in Fig. 3 for four different zenith angles. The normalization or energy scaling can be taken into account by a relation of the following form:

$$N_\mu = N_0 E^\beta \quad (1)$$

where N_0 and β are constants for a given model and mass composition as shown in Table 1.

Fluctuations can enhance trigger rates for air showers produced by lower energy primaries because of the steep cosmic ray spectrum [21]. The fluctuations to high number of particles allow the more numerous low energy showers to trigger. We have studied muon number fluctuations at ground level and how they depend on shower development (mean muon production height) and average muon energy. We have found that the mean energy correlates strongly with production height but that most of the number density fluctuations can be accounted for by fluctuations in the total muon number. This is mainly due to fluctuations in the neutral to charged pion ratios in the first interactions. According to the results shown in Table (1) of Paper I it is sufficient to implement a 20% RMS fluctuation in the average total muon number as obtained with Eq. 1.

Although the actual distributions obtained with simulation do show a long tail to low muon numbers (up to a factor of 4 reduction), such showers are not expected to be relevant for triggering the array precisely because they have so few muons. As a result it is sufficient to assume a gaussian distribution.

4 Detector simulation

4.1 The Haverah Park Array

The trigger rate of an air-shower array at large zenith angles is extremely sensitive to the geometry of the array. Factors such as the shape and relative height of detectors become very important for such showers. Figure 4A

Model	A	β	N_μ (10^{19} eV)
SIBYLL	1	0.880	$3.3 \cdot 10^6$
	56	0.873	$5.3 \cdot 10^6$
QGSJET	1	0.924	$5.2 \cdot 10^6$
	56	0.906	$7.1 \cdot 10^6$

Table 1: Relationship between muon number and primary energy for different models and primary masses (see equation 1).

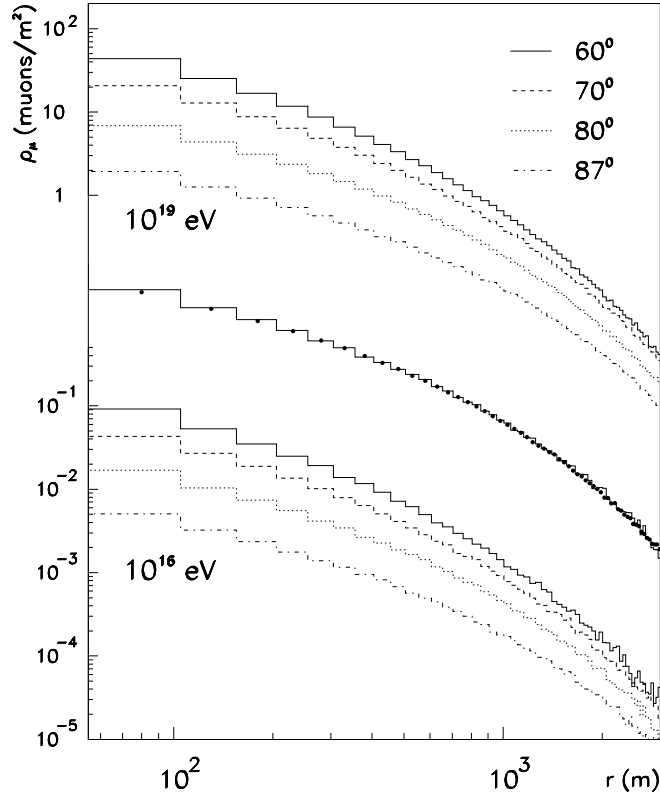


Figure 2: Lateral distribution functions for primary protons of energy 10^{16} eV compared with that for 10^{19} eV protons for zenith angles of 60° , 70° , 80° , and 87° using SIBYLL. The two lateral distribution functions plotted in the centre of the figure are from 80° showers of 10^{16} eV (histogram) and 10^{19} eV (dots) normalized using the relationship given in table 1 to emphasize the very close similarity in shape.

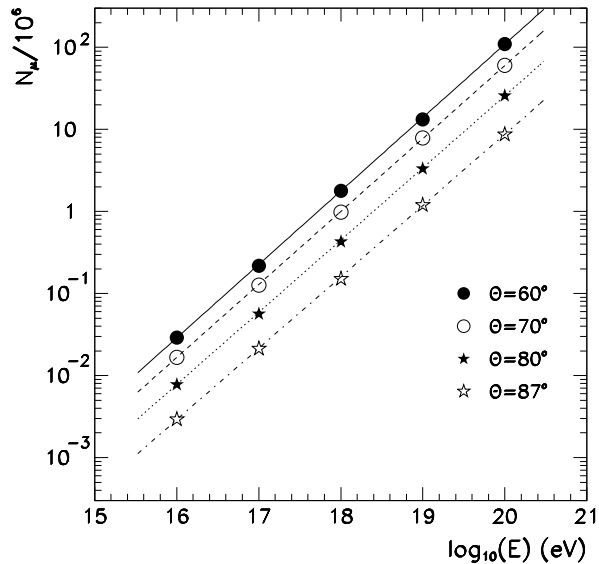


Figure 3: The relationship of total muon number to primary energy for protons of four zenith angles using the SIBYLL model.

shows the layout of the Haverah Park array. The relative heights and orientations of the four A-site detectors, the triggering detectors, are shown in figure 4B. A gradient across the array is apparent and this has a significant effect on the observed azimuthal distribution (see section 6). Figure 4C shows the positions of individual tanks within a detector hut. The signals from 15 of the 16 tanks, each of area 2.25 m^2 , were summed to provide the signal used in the trigger. One tank in each hut was used to provide a low gain signal. See [12] for a more detailed description of the array.

Water-Čerenkov densities are expressed in terms of the mean signal from a vertical muon (1 vertical equivalent muon or VEM). It has been shown that this signal was equivalent to approximately 14 photoelectrons (pe) [22].

The formation of a trigger was conditional on: 1. A density of $>0.3 \text{ VEM m}^{-2}$ in the central detector (A1) 2. At least 2 of the 3 remaining A-site detectors recording a signal of $>0.3 \text{ VEM m}^{-2}$.

The rates of the triggering detectors were monitored daily. Over the life of the experiment, after correction for atmospheric pressure effects, the rates of the detectors were stable to better than 5%.

4.2 Čerenkov signals of vertical particles

The calculation of the water-Čerenkov signal from horizontal showers is complex. It is informative to consider first the simpler case of vertical showers. A GEANT simulation of the propagation of vertical electrons, gammas, and

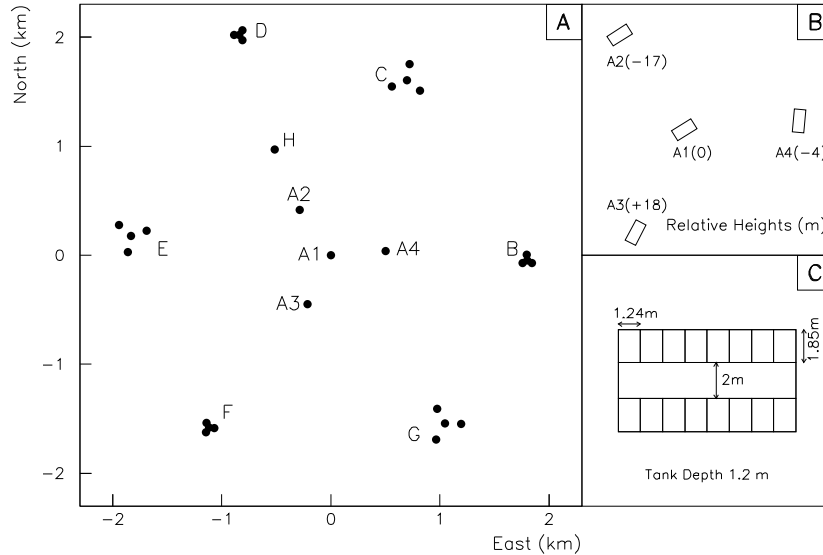


Figure 4: The Haverah Park Array. A) The 2 km array. B) The relative heights and orientations of the A-site detector huts. C) The arrangement of water tanks within an A-site detector hut.

muons through Haverah Park tanks has been performed (WTANK [20]). The wavelength dependences of the physical properties of the tank have been taken from [20] but normalised to the following peak values which are the best estimates for the Haverah Park tanks:

- reflectivity of the walls - 83%
- absorption length of the water - 15 m
- photomultiplier (PMT) quantum efficiency - 22%

The Thorn/EMI, 9618 PMT wavelength acceptance function is taken from the manufacturers specifications.

The results of this simulation are summarized in figure 5. It can be seen that the values used enable us to reproduce the measured signal from an average vertical muon (assuming a mean muon energy of 1 GeV [4]).

The signal from a vertical muon is composed primarily of the Čerenkov light emitted from the muon track. However there is a significant contribution from Čerenkov light emitted by δ -ray electrons (2 pe of the 14 pe total for an average vertical muon).

By contrast the mean energy of electrons and gamma-rays in vertical showers is below 10 MeV. Convolving the energy spectrum of electrons and gammas with the response given by figure 5, we find mean signals of 2.6 and 0.9 photoelectrons for electrons and gamma-rays respectively.

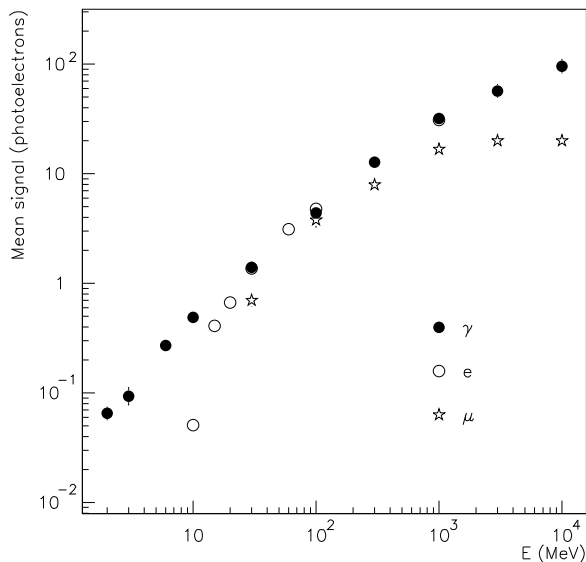


Figure 5: The mean signal produced in a Haverah Park tank by vertical electrons, muons, and gammas as a function of energy (low energy electrons are absorbed in the lid of the tank).

4.3 Signals produced by horizontal showers

Three factors complicate the picture for horizontal showers. Firstly for horizontal showers it is possible for Čerenkov photons to fall directly onto the PMT without reflection from the tank walls (we refer to such photons as “direct light”). Secondly the azimuthal asymmetry of the Haverah Park tanks (and detector huts) becomes increasingly important at large zenith angles. Thirdly the mean muon energy grows with zenith angle. For 87° showers the mean muon energy is 200 GeV. For higher energy muons the probability of interaction in the tank is much greater. The production of secondary electrons via pair-production, bremsstrahlung, nuclear interactions (collectively referred to as PBN interactions), and electron knock-on (δ -rays) is therefore enhanced. For example the correction due to δ -ray production increases from 2 pe at typical vertical muon energies of 1 GeV to around 3 pe for > 10 GeV.

Signal enhancements due to direct light and muon interactions appear in only a fraction of events and hence do not greatly affect the peak of the photoelectron distribution. They do however add long tails to this distribution which are of great importance in calculation of the array trigger rate. Figure 6 shows the different contributions to the water-Čerenkov signal of a horizontal muon as a function of energy. A single Haverah Park tank is considered with muons propagating parallel to the short (1.24 m) side of the

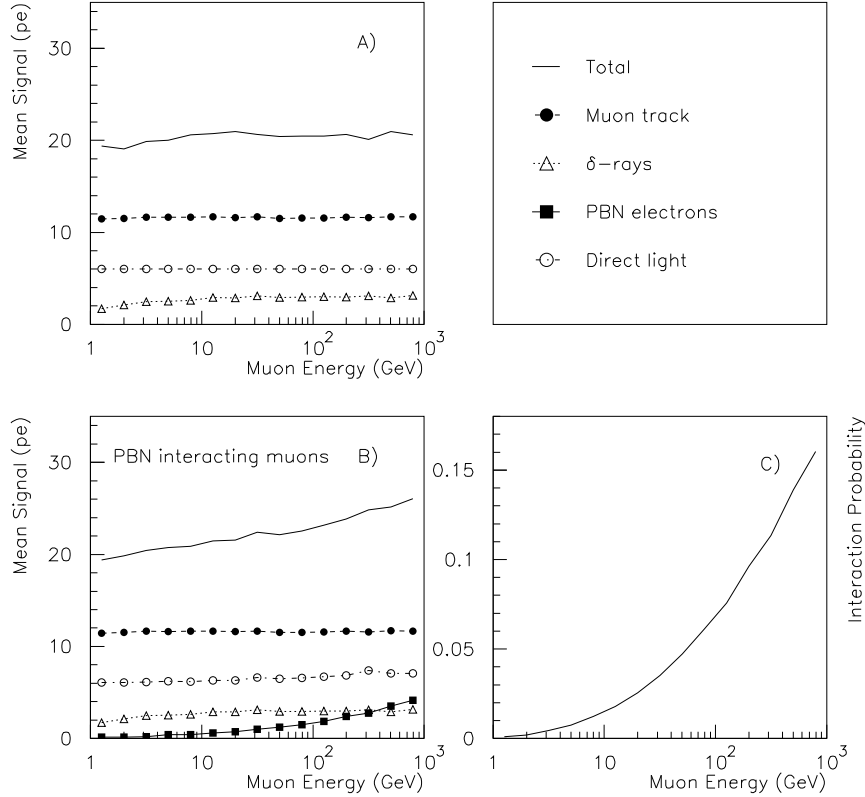


Figure 6: The different contributions to the total signal produced by horizontal muons. A) The mean signal produced by those muons not undergoing PBN interactions in the tank. B) The mean signal produced by PBN interacting muons C) The probability of a muon undergoing a PBN interaction as a function of energy.

tank.

For showers of $> 60^\circ$ the electromagnetic component is almost entirely a product of muon decay as explained in section 2. Convolving the number and energy spectrum of electrons and gammas with the tank response shown in figure 5 we find that the electromagnetic component contributes 2.8 pe for each muon corresponding to 20 ± 2 % of the vertical equivalent muon signal.

5 Implementation

We have simulated the rate of the Haverah Park array as a function of the zenith angle following the steps described below. First of all we simulated 100, 10^{19} eV, showers for zenith angles from 60° to 88° in steps of 2° , without magnetic field, for each of the four combinations of primary mass and

interaction model as described above. Use is made of the ideas developed in Paper I.

For each zenith angle the following procedure is applied:

1. The inputs of the analytical model (LDF, $\mathcal{E}(r)$ and $\langle d \rangle$) are parameterized.
2. The analytical model is applied to these parameterizations to generate muon density maps of the showers in the transverse plane taking into account magnetic field effects.
3. The density maps for different primary energies are obtained with the energy scaling relationship given by Eq. 1 and the parameters shown in Table 1.
4. Different azimuthal angles are considered by simple rotation algorithms in the approximation explained in section 3 of Paper I.

For each of these zenith angles we have calculated the triggering probability of the Haverah Park array in 40 energy bins between 10^{16} eV and 10^{20} eV and 18 azimuth bins as follows:

1. The shower is directed on to the array N times with random core locations on the ground plane up to X km from the centre of the array. N and X are varied according to the primary energy and zenith we are dealing with. Typical values are $N = 10000$ and $X = 8$ km.
2. Each time a shower is directed at the array, the total muon number (N_μ) is fluctuated with a gaussian distribution of spread $0.2N_\mu$ to take into account shower fluctuations.
3. The density in the ground plane at the location of each of the trigger detectors is read from the muon density maps with an appropriate projection, taking into account the corrections due to the different heights of the detectors and the effects of the magnetic field as explained in section 7 of Paper I.
4. The corresponding signal in each of the trigger detectors is generated (see next subsection).
5. The trigger condition of the Haverah Park array is tested.
6. If an event is deemed to trigger the array then the primary energy and the combination of detectors contributing to the trigger are recorded.

The triggering probability derived in this way has been convolved with a primary energy spectrum [23], derived from Akeno and Haverah Park data, to obtain the event rate at each zenith and azimuth angle. The final step

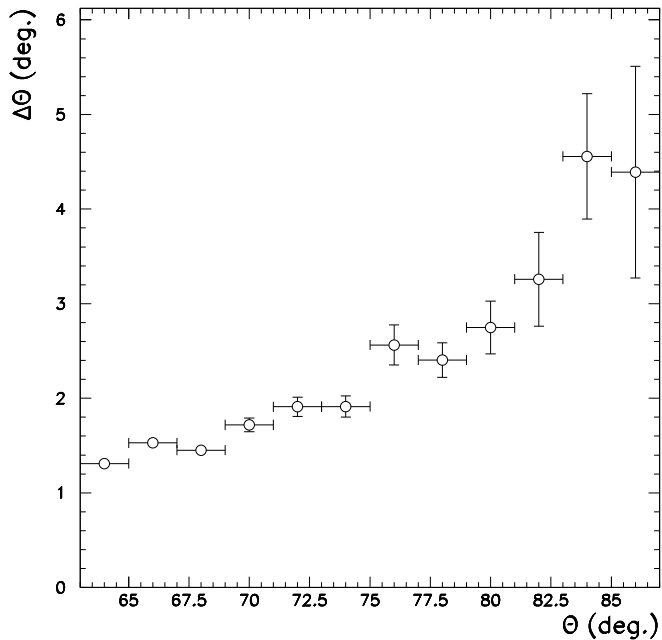


Figure 7: The uncertainty in reconstructed zenith angle as a function of zenith angle.

before comparison with data is to convolve the obtained zenith angle distribution with the appropriate measurement errors. The arrival directions of all the data that had zenith angle greater than 60° have been reanalysed assuming a plane front for the muons and using all available timing information. Previously only times from the four central triggering detectors were used to compute the arrival directions [24]. Here up to 16 times were used in the analysis with the additional data being from the detectors ~ 2 km from A1 in the ground plane. The uncertainty in arrival direction for each event has accordingly been significantly reduced. Fig. 7 shows the average uncertainty in zenith angle of the reconstructed events as a function of zenith angle. The uncertainty in azimuth angle is approximately constant and is $\sim 1^\circ$. The events considered here have not been analysed for core position. Accordingly some of the very large zenith angle events may have fallen a long way outside the boundary of the array and consequently have a larger uncertainty in zenith angle than suggested by fig. 7.

We have rejected about 3% of the events having an error exceeding 4.5° in the reconstructed zenith angle θ . The RMS error in zenith angle shown in fig. 7 is used to *smear* the calculated distribution.

5.1 Implementation of the signal in detector

The signal is generated as follows:

1. The projected area of the detector in the shower plane is calculated.
2. Given the local muon density and the projected area, we sample the number of incident muons from a Poisson distribution.
3. The track length of each muon through the detector is sampled from a distribution obtained analytically from the detector geometry (see figure 4C).¹
4. The contribution of indirect Čerenkov light from the incident muons and from δ -ray electrons is calculated from the sampled track lengths (12 pe for each 1.2 m of track, with an additional 3 pe/1.2 m to account for the signal from δ -rays as described in the previous section).
5. The signal from direct light on the PMTs is related to the detector geometry in a more complex way and is implemented using WTANK to simulate the passage of muons through the whole detector for a range of zenith and azimuth angles.
6. The probability of PBN interactions in the detector is calculated from the track length and the muon energy (obtained from the $\mathcal{E}(r)$ with a zenith angle dependent correction for the magnetic field).
7. If an interaction is deemed to occur then the energy of the resulting em-cascade is sampled from the appropriate differential cross-section. The signal produced by this cascade is calculated using an analytical approach.
8. The electromagnetic component of the shower is approximated by the addition of 2.8 pe for each muon as discussed in the previous section.

The contributions to the signal depend in different ways on the zenith and azimuth. The mean signal for those contributions proportional to the track are constant with azimuth and zenith, because of the compensating effect of the projected area of the detector. In fact the mean signal is simply proportional to the volume of the detector. For larger zenith angles fewer muons produce the same signal so Poisson fluctuations become more important. The mean signal produced by direct light increases with zenith and has a complex dependence on azimuth. The mean signal from the electromagnetic component is proportional to the projected area, and hence decreases with zenith and has a simpler azimuthal dependence.

¹This distribution accounts for the possibility that a single muon may traverse several tanks.

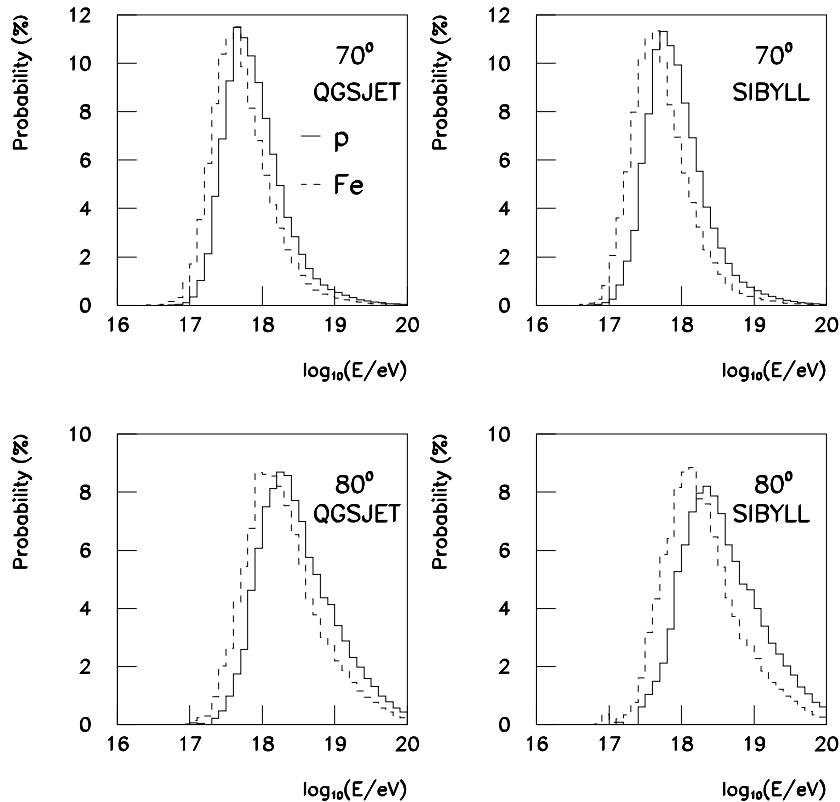


Figure 8: The energy distribution of showers which trigger the Haverah Park array at 70° and 80° for each of the four combinations of model and primary mass composition shown as a probability for each energy bin.

We note that the use of distributions (rather than mean values) for different contributions to the signal is essential for accurate calculation of the event rate.

6 Results and comparison with data

6.1 Energy distribution of showers that trigger the array

In Fig. 8 we show the energy distribution of showers which trigger the array as calculated with the QGSJET and SIBYLL models and for proton and iron primaries at two zenith angles. The mass dependence seen in Fig. 8 is a consequence of the greater number of muons produced by heavier primaries. The choice of interaction model has a somewhat smaller effect on the energy response.

Fig. 9 shows the mean and width of the energy distribution as a function of zenith angle (for QGSJET with proton primaries). The median energy

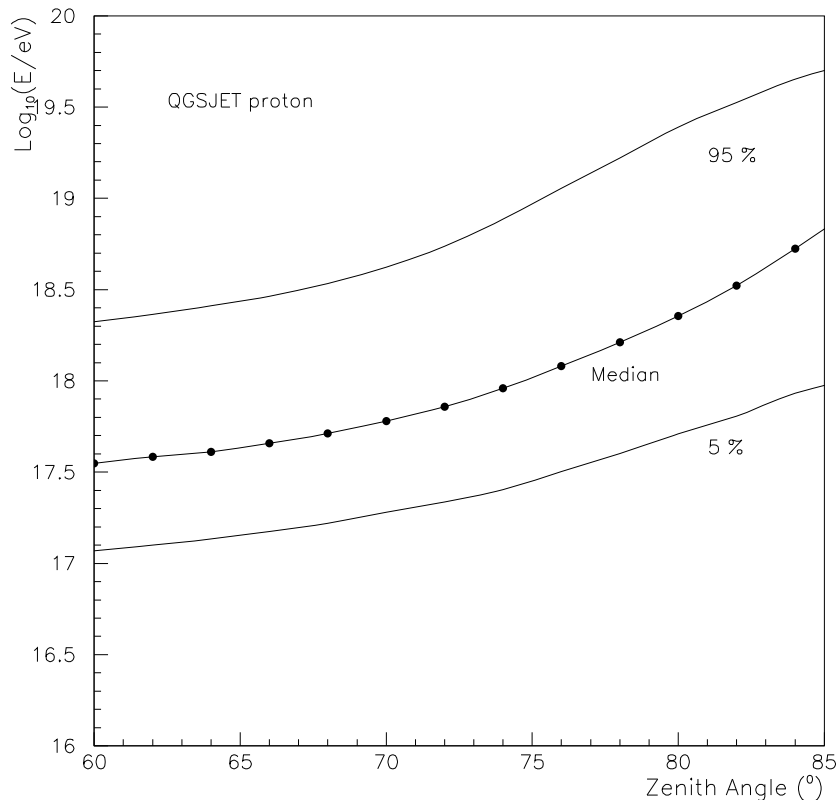


Figure 9: The median and percentiles of the energy distributions of Fig. 8 as a function of zenith angle (QGSJET with proton proton primaries).

changes from $\sim 6 \times 10^{17}$ eV at 70° to $\sim 5 \times 10^{18}$ eV at 84° .

6.2 Azimuthal distribution

One of the most stringent tests for the simulation of horizontal air showers is the prediction of the azimuthal distributions. Minor corrections in the altitude of the detectors, or the orientation of the tanks can lead to large differences in the rates for inclined showers. The total event rate is dominated by events triggering only 3 of the 4 A-site detectors. The azimuthal distribution is best understood by separating these 3-fold events into 3 sets, each set requiring that a particular detector *does not* trigger. The recorded azimuthal distributions for each of these three sets (A2 out, A3 out and A4 out) are shown in Fig. 10. The calculated distributions (using QGSJET with primary protons) are shown normalised to the data for comparison of the shape. The agreement is reasonable with the exception of the set “A2 out”. There are many possible reasons for this disagreement. In particular we will in future consider reflection and absorption in the ground around

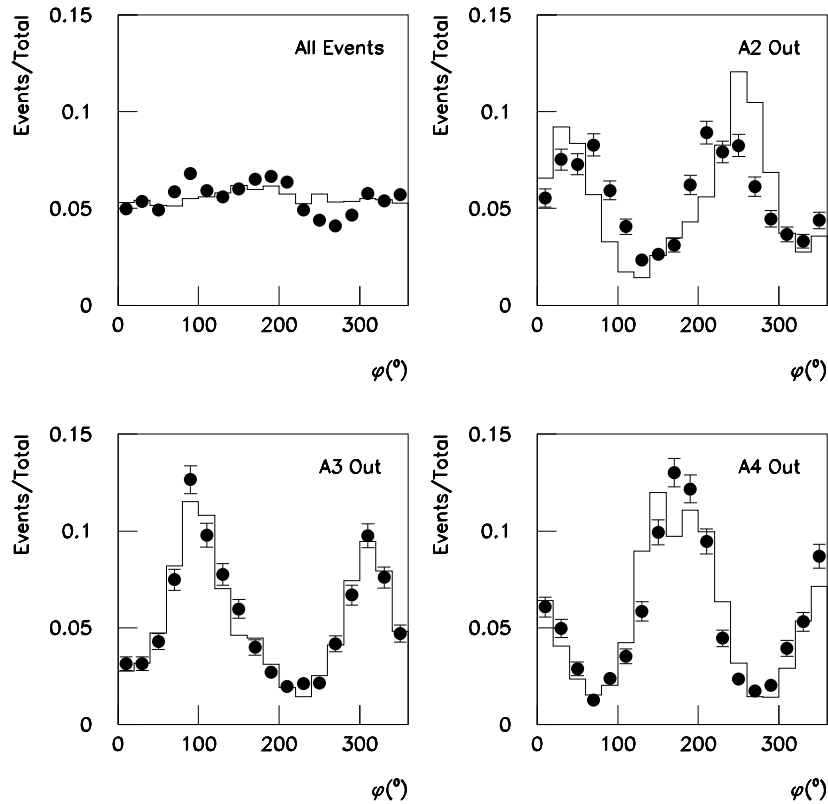


Figure 10: Azimuthal distribution of events recorded above 59° for all events and three sets of three fold events. The distribution of events not triggering each of the A2, A3 and A4 detectors are shown in the later three plots. The simulations use the QGSJET model with proton primaries normalised to the data.

the detectors, but we are encouraged by the overall result.

6.3 Zenith angle distribution

In Fig. 11 we show the contributions to the total rate (from each of the processes considered) as a function of zenith angle. The QGSJET model and proton primaries are assumed. Similar plots for other hadronic models and primaries differ mainly in their normalization. It should be noted that inclusion of only the muon track contribution would lead to underestimating the total rate by a factor ~ 3 (~ 4) at 65° (85°). The effects of delta rays, direct light, electromagnetic corrections, and pair production and bremsstrahlung are all very significant in the calculation of the overall rate. The effect of fluctuations in the total muon number in a shower represents at most a 20% rate enhancement because of the large width of the energy response at a

given angle.

The left hand plot of Fig. 12 shows the number of events detected at Haverah Park as a function of the zenith angle compared to the expected number of events for two different models and two mass compositions. The error bars on the data points are statistical. The right hand plot illustrates the effect of the uncertainty in the primary energy spectrum on our result. The maximum and minimum predictions from the spectrum described in [23] (using one sigma errors) are shown together with the result obtained using the primary spectrum parameterized in [17] (all for proton primaries using the QGSJET model).

We stress that no normalization was done with the simulated events. The shape of the simulated distribution is in good agreement with data between 60° and 70° while at higher zenith angles there is a mild disagreement, at most a $\sim 30\%$ effect. Within the uncertainties resulting from the zenith angle measurement, the primary mass, the interaction models and the primary energy spectrum, the simulated overall rate of showers above 60° is completely consistent with the data.

For most assumptions of primary spectrum and interaction model an intermediate primary mass in the decade around 10^{18} eV seems to be required to fit the data. Further work is in progress to select higher energy events by considering detectors (B – H of Fig. 4A) that are not in the trigger. For example the event discussed in [7] and believed to be of energy $\sim 10^{20}$ eV struck 20 of the detectors.

7 Conclusion

We have presented the first comparison of $> 10^{17}$ eV air-shower data above 60° with simulation. The agreement is reasonable and allows us to state that the detection of HAS induced by hadronic primaries in an array of water-Čerenkov tanks can be explained in terms of the muonic component. The effects of all the considered contributions to the tank signals have been shown to be extremely important in understanding the total rate.

Our final results differ from the preliminary ones reported earlier [14] in several respects. We have taken into consideration the electromagnetic component from muon decay separately. Previously this contribution was taken together with the correction due to δ -rays. We have further improved the implementation of the PBN corrections taking into account their increase with the muon energy. We have also simulated the ground number density profiles in a completely different fashion making use of the model described in Paper I.

The general shape agreement between data and simulation both for the zenith angle and azimuthal angle differential rates, together with agreement in the absolute normalization makes us confident that the geometrical con-

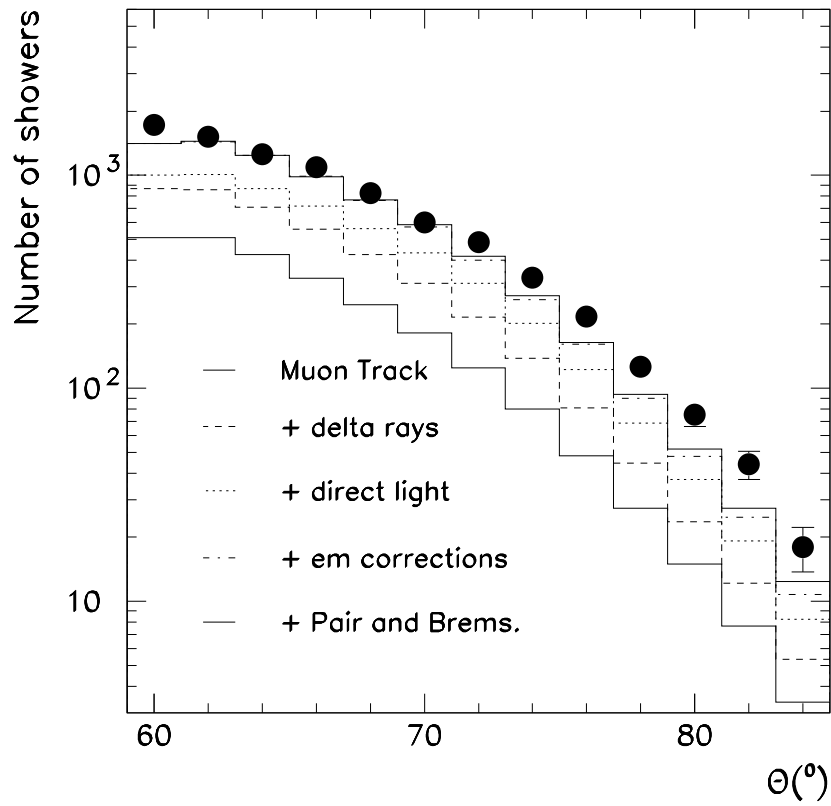


Figure 11: The total number of events recorded by the Haverah Park array as a function of zenith (dots) compared with the prediction obtained using a proton primary composition and the QGSJET model. Different contributions to the total rate are illustrated and are added cumulatively.

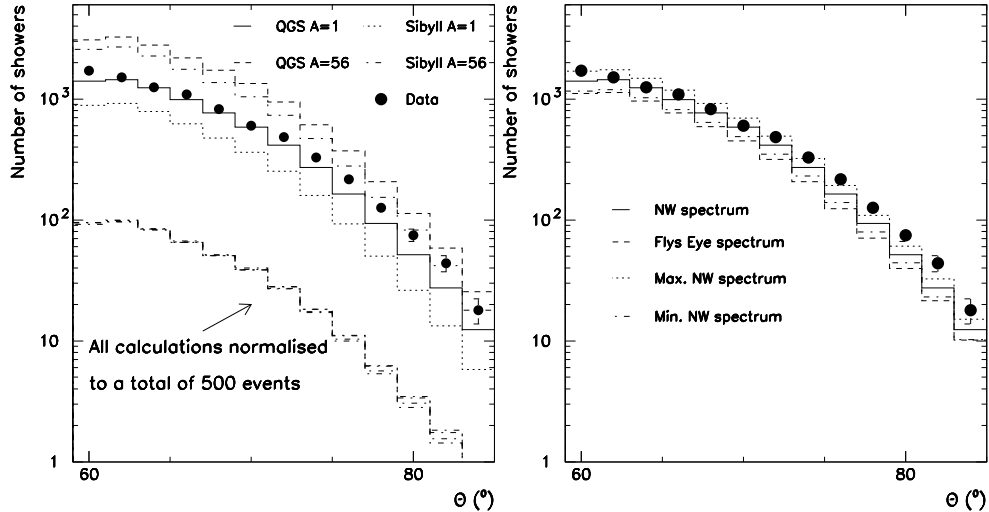


Figure 12: Left panel: A comparison of all four model/mass combinations at the recorded Haverah Park zenith angle distribution. The lower histograms show the calculated rates normalized to illustrate the differences in shape. Right panel: A comparison of the recorded Haverah Park zenith angle distribution for different primary spectra.

siderations have been taken into account correctly, at least at the 20% level. This, together with the general agreement with our preliminary rate simulation, which used Monte Carlo shower simulation rather than the analytical approach described in Paper I, provides strong supporting evidence for this approach as an important tool for HAS studies.

The normalization of the shower rate is sensitive to the model used for high energy hadronic interactions. For proton showers the absolute normalization of the rate differs by up to a factor of two for the two models considered. The absolute rate has also been shown to be very sensitive to the primary composition. There is about a factor 2.2 (3) enhancement, reasonably independent of zenith angle, for the differential rate normalization if the primary particles are assumed to be iron nuclei in the QGSJET (SIBYLL) model. It is interesting to note that current air-shower models are not able to reproduce the observations of high energy particles close to the shower axis above 10^{16} eV [25]. This may be a possible explanation of the $\sim 30\%$ disagreement above 80 degrees (where the surviving muons all originate close to the shower core).

These effects illustrate that HAS measurements may provide another tool with which to study both primary composition and hadronic interactions in ultra high energy cosmic rays. Future detectors such as the Auger Observatories should benefit significantly from the study of cosmic ray showers at

large zenith angles.

Acknowledgements: We thank Xavier Bertou for helping us with the angular reanalysis of the data described in [14] and Gonzalo Parente for suggestions after reading the manuscript. This work was partly supported by a joint grant from the British Council and the Spanish Ministry of Education (HB1997-0175), by Xunta de Galicia (XUGA-20604A98), by CICYT (AEN99-0589-C02-02) and by PPARC(GR/L40892).

References

- [1] Nagano, M. *et al.*, *J. Phys. Soc. Japan* **30** 33 (1971); Mikamo, S. *et al.*, *Lett. al Nuovo Cimento* **34** N 10, 273 (1982); Nagano, M. *et al.*, *J. Phys. G: Nucl. Phys.* **12** 69 (1986); T. Doi, *et al.*, Tokyo U. preprint - ICRR-353-96-04 (1996) 25-28; N. Inoue *et al.* (Agasa Coll.), *Proc. of 26th Int. Cosmic Ray Conf.*, Salt Lake City, (1999) vol.1 p. 361.
- [2] G. Navarra *et al.* *Nucl. Phys. Proc. Suppl.* **B70** (1999) 509-511; M. Aglietta *et al.* *Proc. of 26th Int. Cosmic Ray Conf.*, Salt Lake City, (1999) vol.2 p. 24.
- [3] G.E. Allen *et al.* *Proc. of XXIV Int. Cosmic Ray Conf.*, Rome, (1995) vol.1 p. 321.
- [4] *The Pierre Auger Project Design Report.* By Auger Collaboration. FERMILAB-PUB-96-024, Jan 1996. 252pp.
- [5] J. Capelle, J.W. Cronin, G. Parente, and E. Zas, *Astropart. Phys.* **8** (1998) 321.
- [6] Yu.N. Antonov, Yu.N. Vavilov, G.T. Zatspin *et al.*, *Zh. Éksp. Teor. Fiz.* **32** (1957) 227 (*Sov. Phys. JETP* **5** (1957) 172).
- [7] A.M. Hillas *et al.*, *Proc. of the XI Int. Cosmic Ray Conf.*, Budapest (1969), *Acta Physica Academiae Scientiarum Hungaricae* 29, Suppl. 3, p. 533-538, (1970); D. Andrews *et al.* *Proc. of the XI Int. Cosmic Ray Conf.*, Budapest (1969), *Acta Physica Academiae Scientiarum Hungaricae* 29, Suppl. 3, p. 337-342, (1970).
- [8] E.E. Antonov, L.G. Dedenko, Yu.P. Pyt'ev *et al.*, *Pis'ma Zh. Éksp. Teor. Fiz.* **68** (1998) 177 (*JETP Letts.* **68** (1998) 185).
- [9] A.A. Ivanov *et al.*, *Pis'ma Zh. Éksp. Teor. Fiz.* **69** (1998) 263 (*JETP Letts.* **69** (1999) 288).
- [10] M. Ave, R.A. Vázquez, and E. Zas, Submitted to *Astropart. Phys.* (1999) (Paper I).

- [11] E.E. Antonov, L.G. Dedenko, Yu.P. Pyt'ev *et al.*, *Pis'ma Zh. Éksp. Teor. Fiz.* **69** (1999) 614 (*JETP Letts.* **69** (1999) 650).
- [12] R.M. Tennent, *Proc Phys Soc* **92** (1967) 622.
- [13] M.A. Lawrence, R.J.O. Reid, and A.A. Watson, *J Phys G* **17** (1991) 733.
- [14] M. Ave, R.A. Vazquez, E. Zas, J.A. Hinton, and A.A. Watson. *Proc. of XXVI Int. Cosmic Ray Conf.*, Utah, (1999) vol.2 p. 365.
- [15] N.N. Kalmykov and S.S. Ostapchenko, *Yad. Fiz.* **56** (1993) 105; *Phys. At. Nucl.* **56**(3) (1993) 346; N.N. Kalmykov, S.S. Ostapchenko, and A.I. Pavlov, *Bull. Russ. Acad. Sci. (Physics)* **58** (1994) 1966.
- [16] R.T. Fletcher, T.K. Gaisser, P. Lipari, and T. Stanev, *Phys. Rev.* **D50** (1994) 5710; J. Engel, T.K. Gaisser, P. Lipari, and T. Stanev, *Phys. Rev.* **D46** (1992) 5013.
- [17] D.J. Bird, *et al.*, *Phys Rev* **D71** (1993) 3401.
- [18] AIRES: A System for Air Shower Simulation, S.J. Sciutto, *Proc. of the XXVI Int. Cosmic Ray Conf.* Salt Lake City (1999), vol. 1, p. 411-414; S.J. Sciutto, *preprint archive astro-ph/9911331*.
- [19] E. Zas, F. Halzen, and R.A. Vázquez, *Astropart. Phys.* **1**, 297 (1993).
- [20] J.R.T. de Mello Neto, WTANK: A GEANT Surface Array Simulation Program GAP note 1998-020.
- [21] G. Parente, R.A. Vázquez, and E. Zas, *Proc. of the XXIV Int. Cosmic Ray Conf.* Rome (1995), vol. 1, p. 377-380.
- [22] A.J. Baxter, Ph.D. Thesis University of Leeds (1967).
- [23] M. Nagano and A.A. Watson, *Rev. Mod. Phys.* (in press), July 2000.
- [24] D.M. Edge *et al.*, *J Phys G* **4** (1978) 133.
- [25] T. Antoni *et al.*, *J Phys G* **25** (1999) 2161